Poly-crystalline silicon-oxide films as carrier-selective passivating contacts for c-Si solar cells

Yang, Guangtao; Guo, Peiqing; Procel, Paul; Weeber, Arthur; Isabella, Olindo; Zeman, Miro

DOI
10.1063/1.5027547

Publication date
2018

Document Version
Accepted author manuscript

Published in
Applied Physics Letters

Citation (APA)
Yang, G., Guo, P., Procel, P., Weeber, A., Isabella, O., & Zeman, M. (2018). Poly-crystalline silicon-oxide films as carrier-selective passivating contacts for c-Si solar cells. *Applied Physics Letters*, *112*(19), 1-6. Article 193904. https://doi.org/10.1063/1.5027547

Poly-crystalline silicon-oxide films as carrier-selective passivating contacts for c-Si solar cells

Guangtao Yang[1], Peiqing Guo[1], Paul Procel[1], Arthur Weeber[1,2], Olindo Isabella[1], and Miro Zeman[1]

1. *Delft University of Technology, PVMD group, Mekelweg 4, 2628 CD Delft, the Netherlands*
2. *ECN Solar Energy, PO Box 1, 1755 ZG Petten, the Netherlands*

The poly-Si carrier-selective passivating contacts (CSPC) parasitically absorb a substantial amount of light, especially in the form of free carrier absorption. To minimize these losses, we developed CSPCs based on oxygen-alloyed poly-Si (poly-SiO_x) and deployed them in c-Si solar cells. TEM analysis indicates the presence of nanometer-scale silicon crystals within such poly-SiO_x layers. By varying the O content during material deposition, we can manipulate the crystallinity of poly-SiO_x material and its absorption coefficient. Also depending on O content, the band gap of poly-SiO_x material can be widened, making it transparent for longer wavelength light. Thus, we optimized the O alloying, doping, annealing and hydrogenation conditions. As a result, an extremely high passivation quality for both n-type poly-SiO_x (J_0 = 3.0 fA/cm^2, iVoc = 740 mV) and p-type poly-SiO_x (J_0 = 17.0 fA/cm^2, iVoc = 700 mV) is obtained. A fill factor of 83.5% is measured in front/back-contacted solar cell with both polarities made up of poly-SiO_x. This indicates that the carrier transport through the junction between poly-SiO_x and c-Si is sufficiently efficient. To demonstrate the merit of poly-SiOx layers' high transparency at long wavelengths, they are deployed at the back side of interdigitated back-contacted (IBC) solar cells. A preliminary cell efficiency of 19.7% is obtained with much room for further improvement. Compared to an IBC solar cell with poly-Si CSPCs, a higher internal quantum efficiency at long wavelengths is observed for the IBC solar cell with poly-SiO_x CSPCs, thus demonstrating the potential of poly-SiO_x in enabling higher J_{SC}.

Nowadays, the highest conversion efficiency in crystalline silicon (c-Si) solar cells is enabled by quenching minority carriers' recombination velocity at the c-Si/contact interface by means of carrier-selective passivating contacts (CSPCs). These are technologies based on, for example, a-Si:H (Silicon Heterojunction, SHJ) [1,2,3,4], doped poly-Si [5,6,7], and metal-oxides [8,9,10]. Both SHJ and poly-Si technologies have recently led to world-record, > 26%, interdigitated back-contacted (IBC) solar cells [11,12]. CSPCs based on metal-oxide layers, like MoO_x and TiO_x, are also rapidly emerging and enable efficiencies beyond 22% [8,10]. Nevertheless, there are still restrictions that limit the application of such materials in the PV industry: (i) poly-Si CSPCs are not transparent, especially when heavily doped, because of the high free carrier absorption (FCA); (ii) metal-oxides are transparent, but since standard high-thermal budget metallization influences their work function, carrier selectivity and contacting properties may worsen; (iii) limited transparency and thermal instability also hold in

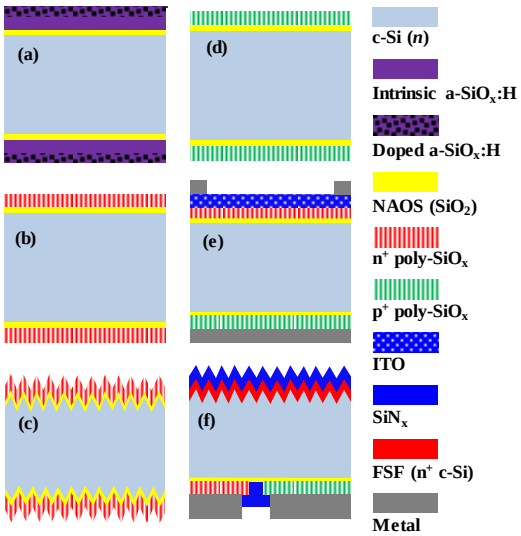

FIG. 1. Schematic illustrations of (a) the PECVD layers that are deposited on both sides of the silicon wafer for passivation test structures and after crystallization with n-type poly-SiO_x on both sides of (b) double-side polished wafer and (c) double-side textured wafer, and (d) with p-type poly-SiO_x on double-side polished wafer; (e) front/back-contacted (FBC) solar cell with ITO capping on the front side and (f) interdigitated back-contact (IBC) silicon solar cell with n-type and p-type poly-SiO_x polarities.

SHJ cells. In fact, parasitic absorption in the amorphous layers results in lower Jsc and commonly-used high-temperature contact firing will be detrimental for the cell efficiency. Therefore, materials like poly-SiO_x have been proposed as CSPCs for solar cell applications [13,14,15,16]. In fact, by varying the content of oxygen atoms in the poly-Si matrix, which will widen the optical band gap of the material, the transparency of the resulting poly-SiO_x increases. Simulation results suggested that by replacing the poly-Si with poly-SiO_x layers within the solar cells, strong band bending is attainable. This is mainly due to the enhanced built-in voltage at the n/p^+ interface, when the p^+ poly-Si is replaced by the wider bandgap p^+ poly-SiO_x layer (increasing the valence band energy). Therefore, an improved carrier selectivity is expected. Moreover, by engineering the in-diffused doping profile at c-Si/poly-SiO_x interface, which enhances carrier lateral transport, the application of TCO layers for carrier extraction can be avoided [16].

In this letter, we show the development of highly-transparent, high-temperature stable poly-SiO_x CSPCs, and their application in various solar cell architectures. They are prepared by alloying oxygen within thin a-Si:H film during the thin-film silicon deposition with plasma enhanced chemical vapor deposition (PECVD). After high-temperature annealing, these amorphous films become poly-crystalline. The deposition conditions and their influences on the optical and electrical properties of the materials are here discussed. As demonstrators, the developed materials are then deployed in front/back contacted (FBC) and IBC solar cells.

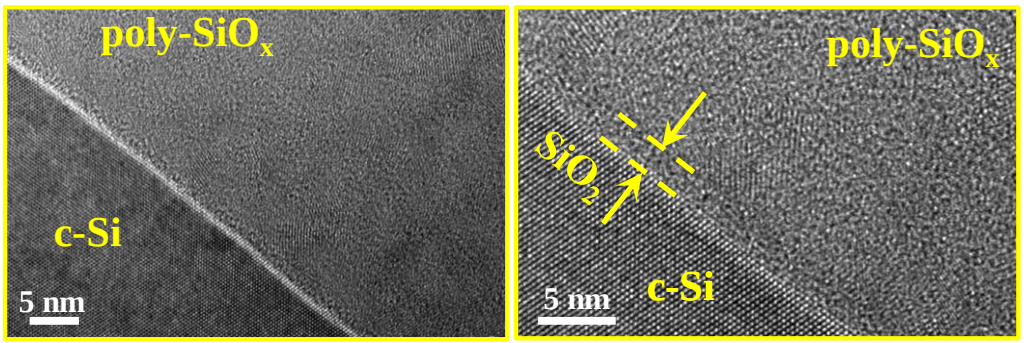

FIG. 2. Transmission electron microscopy (TEM) images of a P-doped poly-SiO_x passivating contact. The ultra-thin SiO_2 tunnelling layer is visible between the c-Si bulk and the poly-SiO_x film.

For all the experiments performed in this work, we used n-type FZ c-Si wafers (thickness: 280 ± 20 µm thick, orientation: <100>, resistivity: 1 ~ 5 Ω cm). Focusing on sample fabrication, the c-Si wafer is first cleaned in HNO_3 (99%), to remove eventual organic contaminations, and then in HNO_3 (68%, at 110 ºC) to remove inorganic contaminations. A dip in 0.55% HF is used to remove the SiO_2 layer grown during such cleaning steps. Then, a fresh ultra-thin SiO_2 layer is formed on each side of the c-Si wafer by nitric acid oxidation of silicon (NAOS). The a-SiO_x:H alloys deposited on top contains two separate layers that are deposited at 180 ºC by PECVD, which are an intrinsic a-SiO_x:H layer capped with a doped a-SiO_x:H layer. For solar cell purposes, the total thickness of such stack is kept as 35 nm. PH_3 or B_2H_6 gases are used as doping sources for the doped layers. Structure of a typical as-deposited sample is shown in FIG. 1(a). A subsequent high temperature annealing, operated at 850 °C, is used to crystallize the materials and drive-in the dopants into the intrinsic SiO_x layer beneath. Structures of symmetrical test samples on double-side polished (DSP) or double-side textured (DST) wafers are shown in FIG. 1(b, c, d). The FBC cell with structure as shown in FIG. 1(e) is prepared with a sputtered Indium-Tin-Oxide (ITO) on the front side, and e-beam evaporated Al on both sides. The IBC solar cell, with its structure shown in FIG. 1(f), is processed with the already developed process, described in our previous work [7].

Transmission electron microscopy (TEM) was used to evaluate the structure of doped poly-SiO_x after the annealing. As shown in FIG. 2, nanometer-scale (around 10-nm) crystals are observed within the poly-SiO_x, which are, in most cases, contacted with each other and surrounded by an amorphous tissue. A thin SiO_2 layer of around 1.4 nm is located between the poly-SiO_x layer and the c-Si bulk. About 40 TEM pictures were made and in none of them pinholes are observed.

The oxygen content in poly-SiO_x layers is closely related to their micro-structure and opto-electrical properties. In this work, we varied the oxygen content through the gas ratio R, with $R = [CO_2] / ([CO_2] + [SiH_4])$, during the a-$SiO_x$:H layers PECVD depositions. The same R was however kept constant for both intrinsic and doped materials. As it can be observed in the Raman spectra reported in FIG. 3, the crystallinity of poly-SiO_x films after annealing at 850 °C lowers as R increases. This decrease in crystallinity is ascribed to higher alloying with oxygen, which in turn increases the fraction of the SiO_x amorphous matrix in the layer. Optically, the poly-SiO_x material exhibits lower absorption coefficient for higher R (see FIG.

4). Compared to the formerly developed phosphorous ion-implanted LPCVD poly-Si[17], the absorption coefficient of the PECVD deposited in-situ n-type doped poly-Si [poly-SiO_x material with no oxygen alloying (R = 0)] is higher over nearly the whole wavelength range. Compared to c-Si, considering such additional absorption, we speculate that a higher doping level is achieved within the PECVD in-situ doped poly-Si layer, which results in a more severe FCA. In any case, both LPCVD and PECVD doped poly-Si layers exhibit very high absorption over the long wavelength range near the band edge. FCA in poly-SiO_x layers decreases with increasing R. When the alloying with oxygen is high enough, the optical band gap of poly-SiO_x is widened and the absorption coefficient in the long wavelength region becomes lower than that of c-Si bulk material. This indicates that the materials can be made transparent for longer wavelength light.

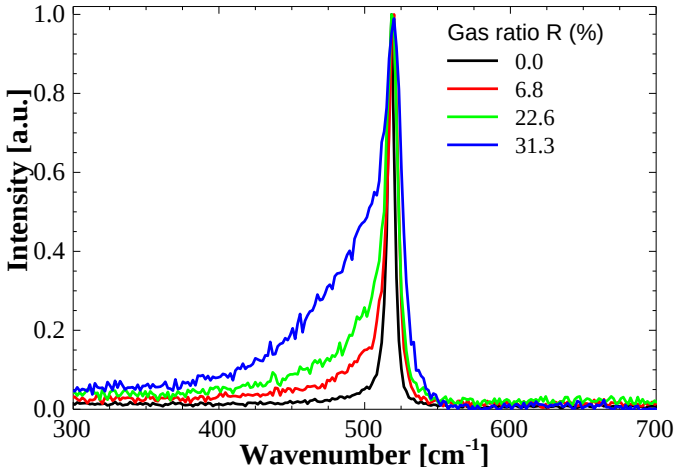

FIG. 3 Raman spectra of 100-nm thick poly-SiO_x layers deposited on quartz glass after annealing at 850 °C for 30 minutes. The gas ratio R (R = $[CO_2]$ / ($[CO_2]$ + $[SiH_4]$)), is varied during the PECVD deposition of a-SiO_x:H layers.

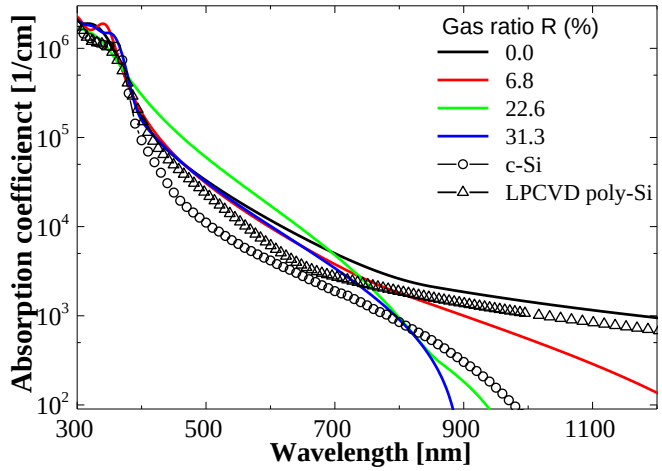

FIG. 4 Absorption coefficient of n-type poly-SiO_x layers deposited on quartz glass with different gas ratio R, but the same doping level. Absorption coefficient curves of LPCVD poly-Si material [7] and c-Si bulk are plotted as references.

In this work, we optimized the electrical properties of poly-SiO_x CSPCs by varying (i) the thickness combination between intrinsic and doped a-SiO_x layers, while keeping the total thickness to be 35 nm, (ii) the doping level of the doped layers, (iii) the gas ratio R during the deposition, (iv) the temperature and time of the annealing step. We find that these parameters are correlated to each other, when pursuing the right balance between passivation and conductivity eventually exhibited by optimized poly-SiO_x CSPCs. For example, the doping profile of the poly-SiO_x CSPCs can be controlled by tuning the doping level of the doped a-SiO_x layer. However, also the annealing temperature and time play a role in the resulting doping profile, which eventually affects the passivation quality of the material [7]. The passivation quality, resulting from optimized conditions on deposition and annealing, for both n-type and p-type poly-SiO_x on double side polished (DSP) wafers, and n-type poly-SiO_x on double side textured (DST) wafer are listed in Table 1. Compared to previously developed

poly-Si CSPCs [7], the n-poly-SiO_x on DSP sample shows a higher iV_{OC} (740 mV), and lower J_0 value (3 fA/cm^2). An iV_{OC} of 718 mV was also obtained for n-type poly-SiO_x deposited on DST wafer, enabling its application on the front side of FBC solar cells for higher J_{SC}. In case of p-type poly-SiO_x, an iV_{OC} of 700 mV was obtained, which deserves further optimization, especially when compared to the passivation quality of the p-type poly-Si counterpart. In order to evaluate the contacting properties of the developed poly-SiO_x layers, the transmission line method (TLM) was deployed to measure the contact resistivity, ρ_C, of Al to doped poly-SiO_x / thin SiO_2 layer / c-Si stack. The ρ_C values of both n-type and p-type poly-SiO_x materials are lower than 1 mΩ·cm^2, which are comparable to those of their poly-Si counterparts (see measured values in TABLE 1).

TABLE 1. Passivation properties of poly-SiO_x carrier-selective passivating contacts on double-side polished (DSP) or textured (DST) c-Si wafers, and the contact resistivity values. As references, the passivation and contacting properties poly-Si passivating contacts are also listed[7].

CSC	surface	doping	J_0 (fA/cm^2)	iV_{OC} (mV)	$\rho_{C,TLM}$ (mΩ·cm^2)
poly-SiO_x	flat	n-type	3.0	740	0.7
	texture	n-type	11.0	718	~
	flat	p-type	17.0	709	0.5
poly-Si	flat	n-type	4.5	735	0.9
	flat	p-type	11.0	716	0.3

After having obtained high-quality passivation properties and low contact resistivities for both n-type and p-type poly-SiO_x layers, we deployed them on a double side flat FBC solar cell, as depicted in FIG. 1(e). The external parameters of these 2-cm^2 cells were measured by using a class AAA Wacom WXS-156S solar simulator and are summarized in TABLE 2. The calibration cells for both *J-V* and *EQE* measurements were calibrated at the CalLab of Fraunhofer Institute for Solar Energy Systems. Due to the limitation on the lateral conductivity of the poly-SiO_x layers, we applied a sputtered ITO layer on the front side of the cell, as a support layer for carriers' lateral transport and as an anti-reflection layer. Before the metal deposition on the front and back side of the cell precursor, the implied open circuit voltage of 695 ± 5 mV was measured over 4 cells in one wafer. After the e-beam evaporated Al as front and rear metal contacts, the measured cell V_{OC} is 681 mV. We attribute this loss in V_{OC} mainly to defects induced by the e-beam radiation at the cell interfaces and c-Si bulk, and to the edge effect, owing to a relatively small cell area. However, most interestingly, a very high solar cell fill factor (FF) of 83.5% was obtained. This proves that the transport of carriers through the junctions and their following collection through ITO and metal are highly efficient. When the e-beam evaporated Al contacts are replaced with screen-printed Ag contacts, the cell V_{OC} of 701 mV was measured in FBC-2 cell, with the SunsVoc of 713 mV. However, due to the larger cell area and the non-optimized screen-printing process, the cell FF is limited by the low conductivity of the metal fingers.

TABLE 2. The cell parameters for front/back contacted (FBC) and interdigitated back/contact (IBC) solar cells with n-type and p-type doped poly-SiO_x carrier-selective passivating contacts used for both polarizations.

Structure	Voc (mV)	SunsVoc (mV)	Jsc (mA/cm^2)	FF (%)	pFF (%)	η (%)
FBC-1 (2-cm^2)	681	701	33.4	83.5	84.3	19.0
FBC-2 (9-cm^2)	701	713	32.8	62.7	82.8	14.4
IBC (9-cm^2)	650	685	39.3	77.0	82.4	19.7

However, the absorption coefficient of the poly-SiO_x thin films so far developed is still higher than that of c-Si or poly-Si in the short wavelength range (see FIG. 4). This will induce optical parasitic absorption losses in the solar cells when a poly-SiO_x layer is used at the front side. Therefore, it seems logic to apply both n-type and p-type poly-SiO_x layers in an IBC architecture. IBC solar cells with textured front side passivated with an a-Si:H/SiN_x:H stack coating a lightly-doped P-implanted front surface field [18] and with poly-SiO_x CSPCs at both polarities on the rear side achieved a conversion efficiency of 19.7%. Compared to the FBC solar cell, the IBC cell presents both lower Voc and SunsVoc, mainly owing to the non-optimum patterning process which induced defects to the doped poly-SiO_x layers. The FF = 77.0% is limited by (i) the high series resistance because of relatively thin 2-μm thick metal Al fingers and (ii) the abovementioned defects which induced recombination. The latter circumstance is supported by the lower pFF compared to that of the FBC solar cells.

In the IBC solar cells, the short wavelength light will be absorbed near the front side and cannot reach the rear side. In the rear side of the cell, both n- and p-type poly-SiO_x layers are transparent with respect to the long wavelength light. This fact enables minimization of the parasitic absorption losses. Absorption of long wavelength light in the IBC solar cell

depends on reflection at the rear side, parasitic absorption at the rear side (mainly by metal), and absorption in the bulk of Si during multiple passes. With these properties in mind, we will compare our results on IBC solar cells based on poly-SiO_x layers and the same architecture cells with poly-Si layers. Compared to the IBC solar cells with poly-Si CSPCs, in the IBC solar cells with poly-SiO_x CSPCs, the part of longer wavelength light that is not absorbed by the poly-SiO_x layers will (1) be partly absorbed by the metal at the poly-SiO_x/metal interface and (2) be partly reflected from the rear metal of the solar cell and escape from the front side of the cell as reflectance, R. Therefore, at long wavelengths, a lower value is observed in the 1-R-T curve of the IBC solar cell with poly-SiO_x layers compared to the IBC solar cell with poly-Si layers on the rear. In this scenario, a large part of the reflected light from the rear metal contacts will be absorbed by the silicon bulk and contribute to the long wavelength response of the quantum efficiency curve. Indeed, a higher internal quantum efficiency (IQE) is observed at long wavelengths for cells with poly-SiO_x layers than in case of IBC cells with poly-Si layers. However, for the poly-SiO_x IBC solar cells, due to the abovementioned process-induced high recombination on the rear passivating contacts, the response below 1100 nm is lower than that of the poly-Si IBC solar cells. By a further optimized patterning process for poly-SiO_x IBC solar cells, a similar short-wavelength response and higher long-wavelength response in the IQE and EQE curves are expected with respect to the IBC cells based on poly-Si CSPCs.

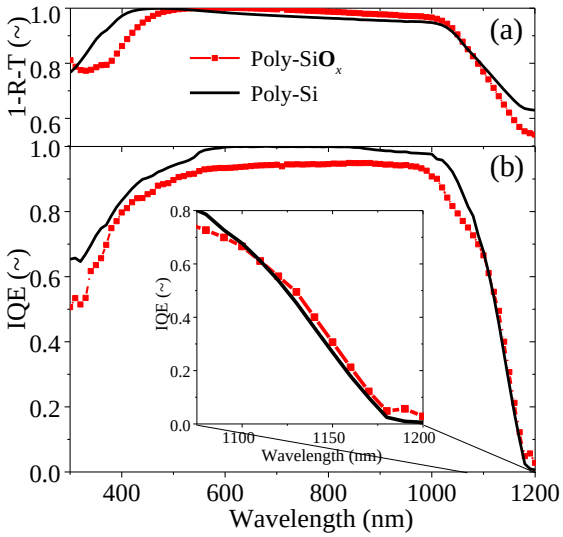

FIG. 5 (a) Reflectance (*R*) and transmittance (*T*) of both cells are plotted as 1-*R*-*T*. (b) The internal quantum efficiency (*IQE*) of the best IBC solar cell with either poly-SiO_x or poly-Si as carrier-selective passivating contacts for both polarities. The inset in (b) zooms-in the long wavelength region.

To conclude, with the aim of minimizing the optical parasitic absorption losses derived from FCA in poly-Si layers when used as CSPCs in c-Si solar cells, we developed the oxygen-alloyed poly-SiO_x materials as CSPCs for c-Si solar cells. By varying the O content and the doping, the crystallinity and the absorption coefficient of the material can be tuned. An excellent passivation is obtained for flat in-situ n-type doped poly-SiO_x (iVoc = 740 mV). P-type poly-SiO_x is more challenging for obtaining a high-quality passivation as high as the n-type counterpart. In fact, the highest iVoc obtained in this work is 700 mV. From contacting point of view, contact resistivity of 0.7 mΩ·cm^2 for n-type, and 0.5 mΩ·cm^2 for p-type are measured. In order to examine the performance of such passivating contact layers within the solar cells, the poly-SiO_x layers are deployed in FBC solar cells as both contact polarities. An ITO layer is applied on the front side to facilitate the carrier's lateral transport and minimize the cell reflection. In first experiments a cell efficiency of 19% for such a simple cell structure is obtained, with a very high cell FF of 83.5%. However, due to the existence of silicon nanocrystals, when such poly-SiO_x is used at the front side of the cell, the absorption at short wavelengths is still substantial, inducing significant optical losses in the solar cell. Due to the band gap widening induced by O alloying, the absorption at longer wavelengths becomes much lower than c-Si bulk. Therefore, these poly-SiO_x CSPCs are used at the back side of IBC solar cells, which cannot be reached by the short wavelength light, and the absorption coefficient of poly-SiO_x layers at long wavelength light is too low to induce (significant) optical losses. Due to the patterning process, induced defects on both the n-type and p-type poly-SiO_x passivating contact fingers, which reduced the cell Voc and FF, a cell efficiency of 19.7% is obtained. However, compared to the IBC solar cells with poly-Si as CSPCs for both polarities, the poly-SiO_x IBC solar cells shows higher IQE

at wavelengths above 1100 nm. This indicates that - for IBC cells - poly-SiO_x CSPCs hold potential in enhancing the cell J_{SC} by maximizing the long wavelength response.

Acknowledgements

This work was carried out with a subsidy of the Dutch Ministry of Economic Affairs (TKI Solar Energy projects) and has received funding from the European Union's Horizon2020 Programme for research, technological development and demonstration under Grant Agreement no. 727523. The authors thank dr. Rudi Santbergen for the fruitful discussions.

References

[1] K. Ding, U. Aeberhard, F. Finger, and U. Rau, Physica Status Solidi: Rapid Research Letter, **6**, 193 (2012).
[2] H. A. Gatz, J. K., Rath, M. A. Verheijen, W. M. M. Kessels, R. E. I. Schropp, Physica Status Solidi A: Applications and material science, **213**, 1932 (2016).
[3] D. Zhang, D. Deligiannis, G. Papakonstantinou, R. A. C. M. M. van Swaaij, and M. Zeman, IEEE Journal of Photovoltaic, **4**, 1326 (2014).
[4] A. Tomasi, B. Paviet-Salomon, Q. Jeangros, J. Haschke, G. Christmann, L. Barraud, A. Descoeudres, J. P. Seif, S. Nicolay, M. Despeisse, S. De Wolf, and C. Ballif, Nature Energy **2**, 17062 (2017).
[5] S. W. Glunz, F. Feldmann, A. Richter, M. Bivour, C. Reichel, H. Steinkemper, J. Benick, M. Hermle, 31st European Photovoltaic Solar Energy Conference and Exhibition, Hamburg (2015).
[6] M. Rienäcker, A. Merkle, U. Römer, H. Kohlenberg, J. Krügener, R. Brendel, R. Peibst, Energy Procedia **92**, 412 (2016).
[7] G. Yang, A. Ingenito, O. Isabella, M. Zeman, Solar Energy Materials and Solar Cells 158, 354 (2016).
[8] J. Geissbühler, J. Werner, S. M. de Nicolas, L. Barraud, A. Hessler-Wyser, M. Despeisse, S. Nicolay, A. Tomasi, B. Niesen, S. De Wolf, and C. Ballif, Applies Physics Letter **107**, 081601 (2015).
[9] X. Yang, Q. Bi, H. Ali, K. Davis, W. V. Schoenfeld, K. Weber, Advanced Materials, **28** (28), 5891 (2016).
[10] X. Yang, K. Weber, Z. Hameiri, S. De Wolf, Progress in Photovoltaics, 25, 896 (2017).
[11] K. Yoshikawa, H. Kawasaki, W. Yoshida, T. Irie, K. Konishi, K. Nakano, T. Uto, D. Adachi, M. Kanematsu, H. Uzu, K. Yamamoto, Nature Energy **2**, 17032 (2017).
[12] https://isfh.de/en/26-1-record-efficiency-for-p-type-crystalline-si-solar-cells/ (accessed 20th of February 2018)
[13] G. Yang, A. Ingenito, O. Isabella, M. Zeman, patent, NLB1 2013722 (2015).
[14] J. Stuckelberger, G. Nogay, P. Wyss, Q. Jeangros, C. Allebé, F. Debrot, X. Niquille, M. Ledinsky, A. Fejfar, M. Despeisse, F.J. Haug, P. Löper, C. Ballif, Solar Energy Materials and Solar Cells, **158**, 2 (2016).
[15] I. Mack,1, J. Stuckelberger, P. Wyss, G. Nogay, Q. Jeangros, J. Horzel, C. Allebé, M. Despeisse, F.-J. Haug, A. Ingenito, P. Löper, C. Ballif, Solar Energy Materials and Solar Cells, (2018), https://doi.org/10.1016/j.solmat.2017.12.030.
[16] O. Isabella, G. Yang, P. Procel, M. Zeman, patent, 2017E00057 NL (2017).
[17] G. Yang, A. Ingenito, N. Van Hameren, O, Isabella, M. Zeman, Applied Physics Letter 108, 033903 (2016).
[18] A. Ingenito, O. Isabella, M. Zeman, Solar Energy Materials and Solar Cells, 157, 354 (2016).